Amino Acids (2010) 39:1463–1475
DOI 10.1007/s00726-010-0611-6

ORIGINAL ARTICLE

Superstoichiometric binding of L-Phe to phenylalanine hydroxylase from *Caenorhabditis elegans*: evolutionary implications

Marte I. Flydal · Tonje C. Mohn · Angel L. Pey · Jessica Siltberg-Liberles · Knut Teigen · Aurora Martinez

Received: 19 January 2010 / Accepted: 27 April 2010 / Published online: 18 May 2010

Abstract Phenylalanine hydroxylase (PAH) catalyzes the hydroxylation of L-Phe to L-Tyr. Dysfunctional PAH results in phenylketonuria and mammalian PAH is therefore highly regulated and displays positive cooperativity for L-Phe (Hill coefficient (h) = 2). L-Phe does not bind to the regulatory ACT domain in full-length tetrameric human PAH and cooperativity is elicited by homotropic binding to the catalytic site (Thórólfsson et al. in Biochemistry 41:7573–7585, 2002). PAH from *Caenorhabditis elegans* (cePAH) is devoid of cooperativity for L-Phe ($h = 0.9$), and, as shown in this work, structural analysis reveal an additional L-Phe binding site at the regulatory domain of full-length cePAH. This site involves the GA(S)L/ISRP motifs, which are also found in ACT domains of other L-Phe binding proteins, such as prephenate dehydratase. Isothermal titration calorimetry further demonstrated 2 binding sites per subunit for cePAH versus ~1 for hPAH. Steric occlusion of the regulatory site, notably by residues Lys215/Tyr216 from the adjacent catalytic domain, appears to hinder regulatory binding in full-length hPAH. Accordingly, the humanized mutant Q215K/N216Y of cePAH binds ~1.4 L-Phe/subunit. This mutant also displays high catalytic activity and certain positive cooperativity for L-Phe ($h = 1.4$). Our results support that the acquisition of positive cooperativity in mammalian forms of PAH is accompanied by a closure of the regulatory L-Phe binding site. Concomitantly, the function of the regulatory ACT domain appears to be adapted from amino acid binding to serving the communication of conformational changes among catalytic subunits.

Keywords Allosterism · Enzyme regulation · Binding stoichiometry · Prephenate dehydratase · Evolution

Abbreviations

AAAH	Aromatic amino acid hydroxylases
BH_4	(6R)-L-erythro-5,6,7,8-tetrahydrobiopterin
cePAH	Phenylalanine hydroxylase from *C. elegans*
hPAH	Human phenylalanine hydroxylase
ITC	Isothermal titration calorimetry
MD	Molecular dynamics
PAH	Phenylalanine hydroxylase
PDT	Prephenate dehydratase
TH	Tyrosine hydroxylase
T_m	Midpoint melting temperature
TPH	Tryptophan hydroxylase
wt	Wild type

Electronic supplementary material The online version of this article (doi:10.1007/s00726-010-0611-6) contains supplementary material, which is available to authorized users.

M. I. Flydal · T. C. Mohn · A. L. Pey · J. Siltberg-Liberles · K. Teigen · A. Martinez (✉)
Department of Biomedicine, University of Bergen, Jonas Lies vei 91, 5009 Bergen, Norway
e-mail: aurora.martinez@biomed.uib.no

Present Address:
A. L. Pey
Departamento de Quimica Fisica, Facultad de Ciencias, University of Granada, Av. Fuentenueva s/n, 18071 Granada, Spain

Present Address:
J. Siltberg-Liberles
Department of Molecular Biology, University of Wyoming, 1000 E. University Ave., Laramie, WY 82071, USA

Introduction

Phenylalanine hydroxylase (phenylalanine 4-monooxygenase, PAH), tyrosine hydroxylase (TH) and tryptophan hydroxylase 1 and 2 (TPH 1 and TPH2) constitute the iron- and tetrahydrobiopterin (BH_4)-dependent aromatic amino acid hydroxylase (AAAH) enzyme family (Fitzpatrick 1999; Teigen et al. 2007). Eukaryotic AAAHs are tetrameric and each subunit includes an N-terminal regulatory ACT domain, a catalytic domain and a C-terminal oligomerization domain (Flatmark and Stevens 1999). Phylogenetic analysis places a protozoan PAH close to the ancestor sequence of the AAAHs, thus aiding to define the evolutionary history of this enzyme family (Siltberg-Liberles et al. 2008). PAH catalyzes the hydroxylation of L-phenylalanine (L-Phe) to L-tyrosine (L-Tyr), the first step in the human L-Phe catabolism leading to complete degradation of L-Phe, mostly in liver (Fitzpatrick 2003). Dysfunction of human PAH (hPAH) results in accumulation of L-Phe in blood, which is the pathogenic factor in the genetic disease phenylketonuria (PKU) (Scriver and Kaufman 2001). If untreated, PKU leads to brain damage and mental retardation. On the other hand, L-Phe is an essential amino acid and hence a well-functioning physiological regulation is required to maintain L-Phe homeostasis. The activation by the substrate L-Phe (Flatmark and Stevens 1999; Kaufman 1993) and phosphorylation at Ser16 (Døskeland et al. 1984; Phillips and Kaufman 1984) are main regulatory mechanisms of mammalian PAH activity, and these mechanisms are synergistically reinforced (Døskeland et al. 1984; Kaufman 1993). The natural cofactor 6R-tetrahydrobiopterin (BH_4) negatively regulates the activation by the substrate (Pey et al. 2004; Solstad et al. 2003).

The activation of mammalian PAH by L-Phe is associated to positive cooperativity in the binding of L-Phe (Kaufman 1993; Thórólfsson et al. 2002). The affinity for L-Phe increases with the substrate concentration in a sigmoidal manner (Hill coefficient (h) $\approx$ 2), and this regulatory mechanism is absent in many mutants of PAH associated with PKU (Erlandsen et al. 2004; Gersting et al. 2008). The cooperativity reflects a transition from a low-activity and low-affinity "T" to a high-activity and high-affinity "R" state, with large accompanying conformational changes (Kappock et al. 1995; Shiman et al. 1979; Stokka and Flatmark 2003; Thórólfsson et al. 2003). The molecular basis for the activation in mammalian PAH, and notably the stoichiometry of L-Phe binding and the initial site for the global conformational changes elicited by the substrate have long been matters of discussion. Thus, the cooperative binding has been proposed to occur either to an allosteric/regulatory binding site different to the distant catalytic site (Gjetting et al. 2001; Shiman and Gray 1980; Shiman et al. 1994) or to the catalytic site itself (Martínez et al. 1990, 1993). As a verification of the latter proposal, detailed differential scanning calorimetry investigations demonstrated that L-Phe only binds to the catalytic domain in full-length tetrameric hPAH (Thórólfsson et al. 2002). Accordingly, the activation of mammalian PAH would result from homotropic cooperative binding of L-Phe to the active sites, where allosteric conformational changes are triggered (Stokka et al. 2004; Thórólfsson et al. 2003). However, the regulatory domain of hPAH, when truncated from the catalytic domain, in fact binds L-Phe (Gjetting et al. 2001). Moreover, though little sequence identity remains between the regulatory ACT domain of mammalian PAH and its distant homolog prephenate dehydratase (PDT) (i.e. 20% over 80 residues) (Siltberg-Liberles and Martinez 2009), it is noteworthy that both enzymes contain the motifs GA(S)L/IESRP (Fig. 1). The binding of L-Phe to the isolated regulatory domain of hPAH involves these motifs (Gjetting et al. 2001) and for PDT their role in L-Phe binding has been crystallographically proven (Tan et al. 2008). We recently noticed that comparison of the crystal structures of rat PAH and *C. tepidum* PDT reveals a region in the catalytic domain of PAH (residues 204–216) that might hinder the access of the amino acid to the GA(S)L/IESRP region in the regulatory domain (Siltberg-Liberles and Martinez 2009). In PAH from lower eukaryotes, the L-Phe binding motifs GAL/IESRP are conserved, but the region 204–216 that contacts the regulatory domain presents non-conservative substitutions with respect to the mammalian enzymes (see sequence alignment in Figure S1, supplemental information).

Caenorhabditis elegans PAH (cePAH) is expressed in the hypodermis underlying the cuticle of the nematode (Loer et al. 1999) and we have recently shown that cePAH is involved in the synthesis of a melanin-like pigment (Calvo et al. 2008). CePAH resembles hPAH with respect to most functional and molecular properties but, like PAH form other lower eukaryotes (Bel et al. 1992; Siltberg-Liberles et al. 2008), it lacks the activation and positive cooperative response for L-Phe (Calvo et al. 2008). Comparative sequence and structural analysis of hPAH, cePAH and PDT performed in this work have uncovered a potential binding site for L-Phe (in addition to the catalytic site) in cePAH, involving the GAL/IESRP motifs. This site is not revealed for hPAH. Further, binding analyses in fact showed that the wild-type (wt) cePAH binds a superstoichiometric amount of the substrate ($\sim$2 L-Phe/subunit) compared with stoichiometric binding for the human enzyme. The structural comparisons also revealed that residues 215/216 might be involved in the functional divergence between nematode and mammalian PAH, as also supported by diverge analysis. We, therefore, prepared

Fig. 1 Sequence alignment of ACT domains**.** *Homo sapiens* PAH (SWISS PROT accession code P00439; residues 34–115), *C. elegans* PAH (code P90925; residues 29–115) and *Chlorobium tepidum* PDT (code Q8KBW6; residues 197–280). The GA(S)L and IESRP motifs are *underlined*

a mutant of cePAH, where residues Gln215 and Asn216 are changed to the residues in hPAH (Q215K/N216Y-cePAH). This mutant was stable, displayed some positive cooperativity and bound only ~1.4 L-Phe. Our results provide insights on the allosteric regulation of mammalian PAH by its substrate and aid to understand the different results obtained on the stoichiometry of binding based on measurements with full length enzymes or isolated regulatory subunits. More importantly, our results support that the emergence of positive cooperativity and activation by L-Phe along evolution is accompanied by occlusion of the regulatory L-Phe binding site operative in lower eukaryotes.

Materials and methods

Homology modelling of full-length tetrameric hPAH and cePAH and evaluation of potential binding sites

We have previously constructed structural models of tetrameric hPAH (residues 19–452) by aligning the dimeric crystal structure of rat PAH (comprising residues 19–427, PDB 1PHZ) with the crystal structure of a truncated tetrameric model of hPAH (comprising residues 118–452, PDB 2PAH) (Thórólfsson et al. 2002). These structures do not have resolution for the flexible loop 137–142 which we modeled into the initial chimeric structure based on the loop coordinates in the structure of the catalytic domain of hPAH (PDB 1PAH). Structural alignments were performed based on the complete sequence alignment used for homology modelling considering the positions of Cα atoms of each residue, with the superimpose functionality of Discovery Studio Visualizer v2.5 (Accelrys). The amino acids of the regulatory domain in the chimeric model were then mutated to the corresponding residues in the human sequence using WhatIf (Vriend 1990). Calculation of most probable histidine protonation states, orientation of the asparagine and glutamine side chains to the most energetically favorable orientation and addition of hydrogen atoms to the entire model were performed using the ICM software (ICM, version 3.6. (Molsoft LLC, San Diego, CA)). The initial hPAH model (residues 19–452) was then refined by energy minimization in Amber10 (Case et al. 2008) and the quality of the final structural model was considered satisfactory according to WhatCheck (Hooft et al. 1996). A structural model of tetrameric cePAH was then prepared by using Swiss-Model (Schwede et al. 2003) based upon the refined hPAH model as template. cePAH and hPAH have an overall sequence identity of 56% (Fig. S1). The high sequence identity simplifies the preparation of the alignment for homology modelling, which includes very few short gaps, all in the regulatory domain up to residue 113, where the numeration of residues gets similar for both proteins (Fig. S1). The model returned from SwissModel was protonated and subjected to side-chain optimization by using ICM and energy minimization by Amber10 (Case et al. 2008). The structural quality of the resulting model was confirmed by WhatCheck. The structural models of tetrameric hPAH and cePAH were analyzed by the ICM Pocket Finder (An et al. 2005) in order to search the entire protein surface for potential ligand-binding pockets.

Expression and purification of hPAH, cePAH and Q215K/N216Y-cePAH

The double mutation Q215K/N216Y was introduced in cePAH cDNA on the pMALc2 expression vector (Loer et al. 1999) by site-directed mutagenesis using the QuikChange kit (Stratagene, La Jolla, CA, USA). The primers used for mutagenesis (5′-CATATTCCCACTCCTCC AG*AAAT*ATTGTGGTTTTGGACCTGACC-3′ (mutated bases italicized) and sequencing were provided by MWG Biotech AG (Ebersberg, Germany). Expression and purification of tetrameric hPAH, cePAH and Q215K/N216Y-cePAH were performed essentially as described (Calvo et al. 2008). Protein concentration was measured spectrophotometrically using ε_{280nm} (1 mg/ml) = 1.0 for hPAH and 1.02 and 1.05 cm^{-1} for wt-cePAH and the mutant protein, respectively. The molecular sizes were determined by analytical size exclusion chromatography using a

calibrated 10/30 Superdex 200 column (Amersham Biosciences).

Enzyme kinetic analysis

At standard assay conditions, PAH enzyme activity was measured at 25°C for 1 min using 1–2 μg of the purified tetrameric forms of the enzymes, which were incubated in 100 mM Na-Hepes, pH 7.0, containing catalase (0.04 mg/ml) and 1 mM L-Phe. After 4-min incubation at 25°C, ferrous ammonium sulfate (100 μM) was added, and the reaction was triggered after 1 min by adding BH_4 (75 μM; from Dr. B. Schircks Laboratories) and 5 mM dithiothreitol (DTT). In some experiments aimed to analyze the L-Phe induced activation of the enzyme, activity including the preincubation step with L-Phe was compared with the activity without preincubation, where L-Phe was added together with BH_4. The reaction was stopped after 1 min (standard reaction time) by adding 1% (by vol.) acetic acid in ethanol, ensuring linearity conditions for the determination of the specific activity. To determine the steady-state kinetic parameters for BH_4 and L-Phe, BH_4 was used at 0–200 μM (at 1 mM L-Phe) and L-Phe at 0–2 mM (at 75 μM BH_4). L-Tyr formed was quantified by HPLC and fluorimetric detection. The saturation curves were fitted to hyperbolic (for BH_4) or sigmoidal (for L-Phe) models with Sigma Plot v.9.0 (SPSS Inc., Chicago, IL, USA).

Circular dichroism

Circular dichroism (CD) spectra were collected on a JASCO J-810 spectropolarimeter with 5 μM of either wt-cePAH or Q215K/N216Y-cePAH in degassed Na-Hepes, 200 mM NaCl, pH 7.0 and stoichiometric amounts of ferrous ammonium sulfate. Far-UV (200–260 nm; 1-mm path length) spectrum was acquired at 25°C and thermal denaturation was performed by following the changes in ellipticity at 222 nm in the temperature range 25–70°C with a heating rate of 1°C/min.

Isothermal titration calorimetry

Isothermal titration calorimetry (ITC) was performed in a VP-ITC titration calorimeter (MicroCal Inc.). Enzyme and L-Phe solutions were prepared in 20 mM Na-Hepes, 200 mM NaCl, pH 7.0 and filtered and degassed prior to titration. hPAH (28 μM subunit fusion protein), cePAH (42 μM subunit) or Q215K/N216Y-cePAH (30 μM subunit) were added to the sample cell and titrated with L-Phe (0.9–2 mM stock solutions). The enzymes were subjected to 30–50 injections (5 μl) of L-Phe with a 240-s interval between each injection at 25°C. The final ratio of [L-Phe]/[enzyme subunit] was >5:1. The mean of the heat from the last 5 injections was subtracted from the raw data to correct for experimental heat dilution. Analysis of the binding isotherms by fitting to models for either one or two types of binding sites was performed using the Origin v7 software (OriginLab). Chi-square minimization was performed iteratively to obtain the best-fit parameters.

Functional divergence analysis

Diverge 2.0 (Gu 2001, 2006) was applied to identify type II divergence sites potentially involved in functional changes between the nematode and mammalian clades using standard physicochemical amino acid classification (positively charged, negatively charged, hydrophilic non charged and hydrophobic amino acids) (Gu 2006). Sequence changes in physicochemical character from one clade to another constitute type II divergence sites, and were divided into 2 classes: class 1—radical change in physicochemical character, which is clade specific, and class 2—radical clade specific change, but with some variance within one or both clusters. Class 1 has the highest probability of being involved in a functional change.

Results

The modeled structure of cePAH

There is so far no crystal structure for any of the full-length AAAHs, most probably due to the complex and dynamic nature of their multidomain, tetrameric structure. But satisfactory models can be prepared by combination of the available crystal structures of the different domains, optimization and energy minimization (see "Materials and Methods" and Fig. 2a). The modeled structures of cePAH and hPAH are very similar (RMSD for Cα = 0.9 Å after refinement). We searched for putative ligand-binding sites in the tetrameric structures by using ICM Pocket Finder. As expected, the catalytic binding pockets were found in the catalytic domains and these were ranked highest according to size (~780 $Å^3$) in both structural models. Moreover, in cePAH, but not in hPAH, an additional pocket (~151 $Å^3$) was found close to the interface between the regulatory and catalytic domains lined by the GAL/IESRP motifs (Fig. 2b). The volume increased to 551 $Å^3$ after docking L-Phe based on a structural alignment with the ACT domain of PDT with L-Phe bound (Tan et al. 2008) and further energy minimization. High structural similarity was seen for the L-Phe binding site in the model of cePAH and PDT (Fig. 3) and in both the structures an optimal orientation of residues around the GA(S)L/IESRP motifs to accommodate the aromatic ring of L-Phe is observed. Thus, Tyr240 in PDT (Fig. 3a) and Tyr72 in cePAH

(Fig. 3b) have similar positions with respect to bound L-Phe. Phe242 (PDT) and Tyr208 (cePAH) also create optimal interactions with the ligand ring. The latter residue is substituted by a histidine (His208) in hPAH (Fig. 3c), but the most remarkable difference between cePAH and hPAH close to the GAL/IESRP motifs are residues 215/216 at the solvent-exposed area (visualized with green transparent surface in Fig. 3). The substitutions in hPAH (Lys215/Tyr216) are larger than that in cePAH (Gln215/Asn216) and notably Tyr216 obtrudes the accessibility to the site, providing an explanation for the inability of Pocket Finder to detect a binding site in this area of hPAH. Thus, these analyses further support our earlier prediction that the expected L-Phe site in the regulatory domain (at the GAL/IESRP motifs) might be blocked by residues from the catalytic subunit (Siltberg-Liberles and Martinez 2009). In order to probe the implication of residues 215/216 in regulatory L-Phe binding we set off to prepare and characterize a humanized variant of cePAH at these positions.

Expression and purification of Q215K/N216Y-cePAH: comparative characterization of the catalytic and regulatory properties of hPAH, cePAH and Q215K/N216Y-cePAH

The mutant Q215K/N216Y-cePAH was successfully expressed and purified to homogeneity at comparable yield as wt-cePAH and hPAH. On the basis of analytical size exclusion chromatography at pH 7.0 and protein concentration 0.2–10 mg/ml, the three enzymes eluted with estimated hydrodynamic radii of 55 Å (hPAH), in agreement to previous measurements (Kleppe et al. 1999), 61 Å (cePAH) and 70 Å (Q215K/N216Y-cePAH). These measurements confirm a tetrameric structure for all the proteins, but also indicate that the double mutation increases the hydrodynamic volume of cePAH.

With respect to the enzyme kinetic properties only hPAH seems to require preincubation with the substrate to obtain maximal activity (Table 1). The saturation curves for the PAH activity of the three enzymes as a function of

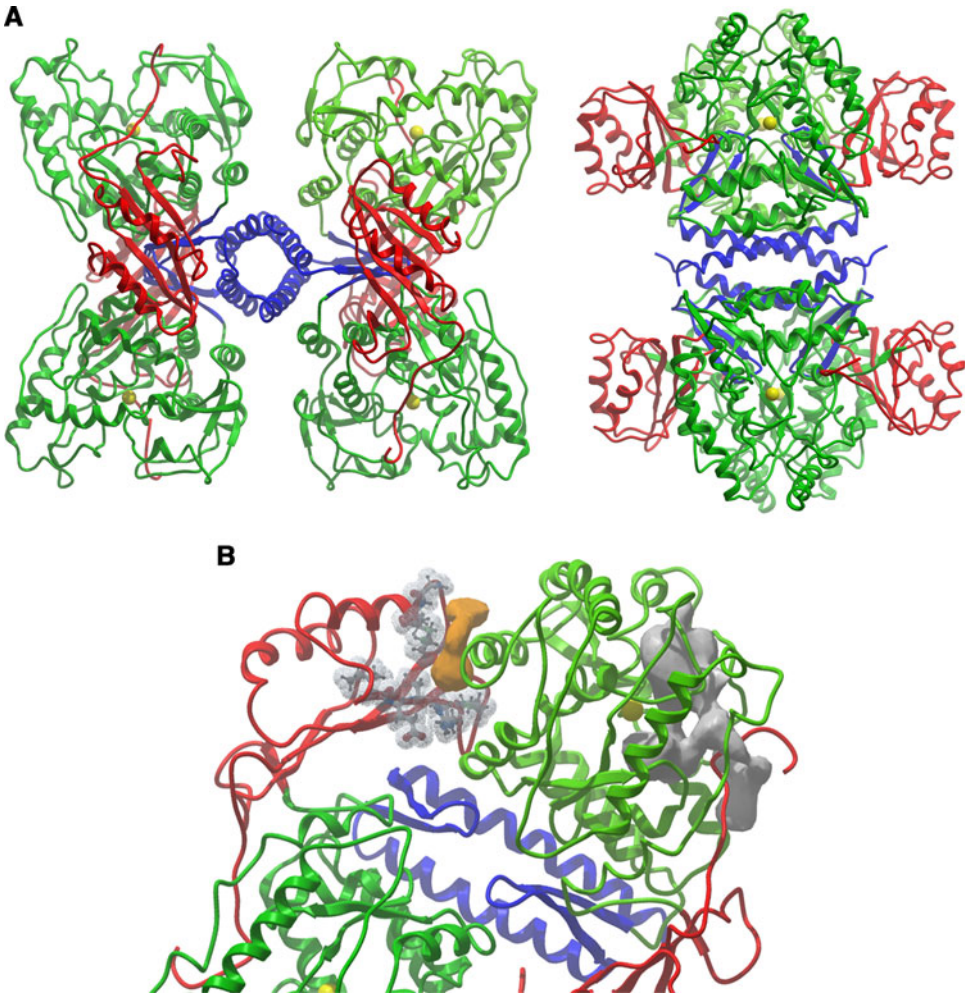

Fig. 2 The modeled structure of cePAH and detection of ligand-binding pockets. **a** Two different views of the ribbon representation of the modeled structure of tetrameric cePAH based on the modeled structure of hPAH (see main text for details). Both backbone structures superimpose with a RMSD for Cα = 0.9 Å. The subunits are colored *red* at the N-terminal regulatory ACT domain, *green* at the catalytic domain with the non-heme iron atom as a *yellow sphere* at the active site and *blue* at the C-terminal oligomerization domain. **b** Putative ligand binding sites in cePAH at the interface between the regulatory (by the GAL/IESRP motifs) and catalytic domains from adjacent subunits (*orange*) and at the active site (*white*) as detected by ICM-pocket finder (color figure online)

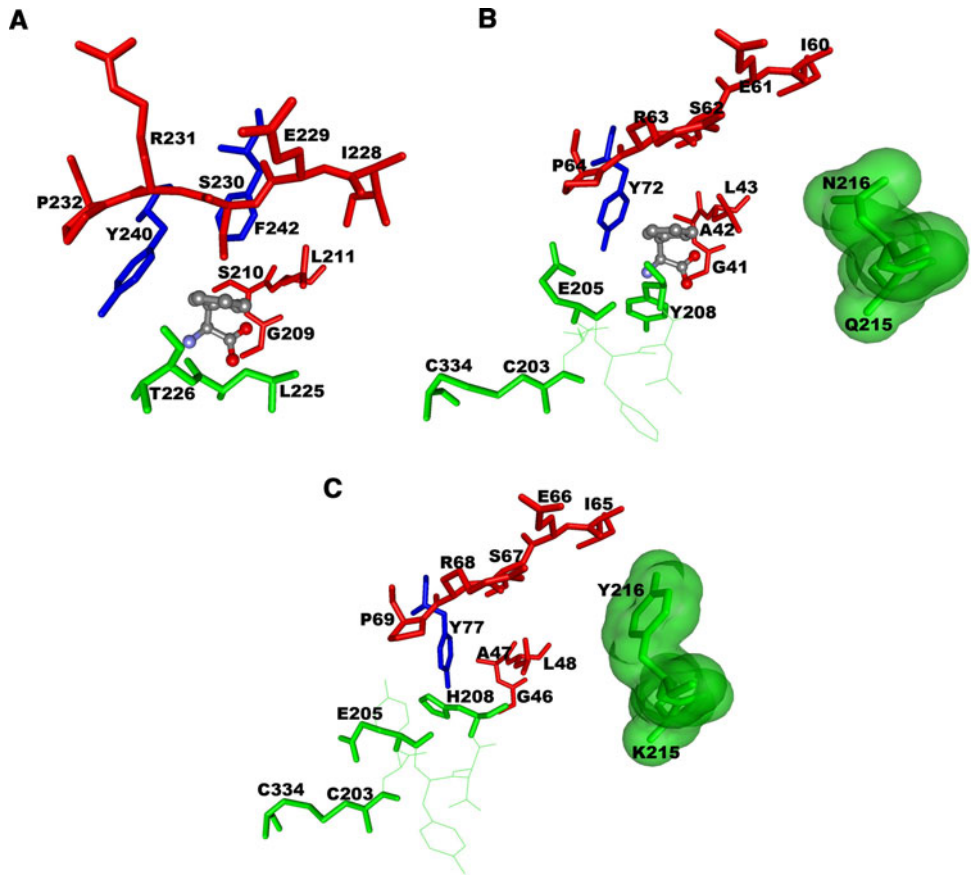

Fig. 3 The regulatory L-Phe binding site in PDT and the putative L-Phe binding site in cePAH**. a** Details of the crystal structure of L-Phe-bound PDT from *C. tepidum* (PDB 2QMX)**.** L-Phe located at the interface between two ACT regulatory domains is shown in *ball* and *stick* representation, GSL/IESRP residues from one domain are shown as *red sticks* and close residues from the same domain in *blue* while those from the adjacent domain in *green*. **b** Detail of the putative L-Phe binding site in cePAH with L-Phe (in *ball* and *stick* representation) docked in the putative binding site (Fig. 2b) with further energy minimization of the docked structure. Residues from the regulatory domain are shown in *red* (motifs GAL/IESRP) or *blue*, and from the adjacent catalytic domain in *green*. **c** The corresponding region in hPAH, with same color code as in **b**. The atoms in the mutated motif (positions 215/N216 in cePAH (**b**) and hPAH (**c**)) are shown with *green* transparent surfaces representing atomic van der Waals radius. See also Fig. S1 (Supplemental information for sequence alignment) (color figure online)

the concentration of substrate and cofactor (Fig. 4 and data not shown) provided the K_m-values (referred to as $[S_{0.5}]$ in the case of cooperativity; Table 1). CePAH completely lacks the characteristic positive cooperativity for L-Phe seen in hPAH ($h \simeq 0.9$ and $\simeq 2$ for cePAH and hPAH, respectively) and Q215K/N216Y-cePAH displays some positive cooperativity ($h \simeq 1.4$) (see the alternative hyperbolic and sigmoidal fittings in Fig. 4, inset). On the other hand, hyperbolic saturation curves were obtained for the activity as a function of cofactor BH_4 concentration for all enzyme forms. Q215K/N216Y-cePAH showed decreased $[S]_{0.5}$ (increased apparent affinity) for L-Phe and higher K_m for the cofactor (Table 1).

Circular dichroism

Circular dichroism (CD) experiments were performed in order to investigate the structural integrity of the Q215K/N216Y mutant compared with wt-cePAH and to obtain information about the thermal stability of the enzymes. The CD spectra of hPAH (Thórólfsson et al. 2003), cePAH and Q215K/N216Y-cePAH (Fig. 5a) show minima at 209 and 222 nm, indicating a high helical content, in agreement with the modeled structure (Fig. 2a) which includes ~38% α-helix. Thermal denaturation experiment monitored by CD (ellipticity changes at 222 nm) (Fig. 5b) revealed similar thermal dependence for the wt and the mutant and further confirmed that the mutation Q215K/N216Y did not significantly perturb the conformational stability of the protein.

Isothermal titration calorimetry (ITC)

The binding of L-Phe to wt and mutant cePAH enzymes comparatively to hPAH was measured by ITC. Good

Table 1 Steady-state kinetic parameters for cePAH, Q215K/N216Y-cePAH and hPAH

Specific activity (μmol L-Tyr/min·mg)				L-Phe[c]			BH_4^c
Enzyme	+L-Phe[a]	−L-Phe[b]	Ratio (+L-Phe/−L-Phe)	V_{max} (μmol L-Tyr/min mg)	h	$[S]_{0.5}$ (μM)	K_m (μM)
cePAH	2.6 ± 0.03	2.1 ± 0.2	1.2	1.9 ± 0.1	0.9 ± 0.1	188 ± 41	29 ± 4
Q215K/N216Y-cePAH	6.5 ± 0.1	4.9 ± 0.1	1.3	6.6 ± 0.2	1.4 ± 0.1	109 ± 9	94 ± 11
hPAH[d]	3.0 ± 0.1	0.7 ± 0.1	4.3	3.5 ± 0.2	1.9 ± 0.2	154 ± 20	33 ± 5

Data are mean ± SEM obtained from nonlinear regression analysis from 3 independent experiments, each performed in duplicate

[a] Measured at standard conditions (1 mM L-Phe and 75 μm BH_4) with L-Phe preincubated enzyme

[b] Measured at standard conditions (1 mM L-Phe and 75 μm BH_4) with non-L-Phe preincubated enzyme

[c] Obtained with L-Phe preincubated enzyme

[d] From (Calvo et al. 2008)

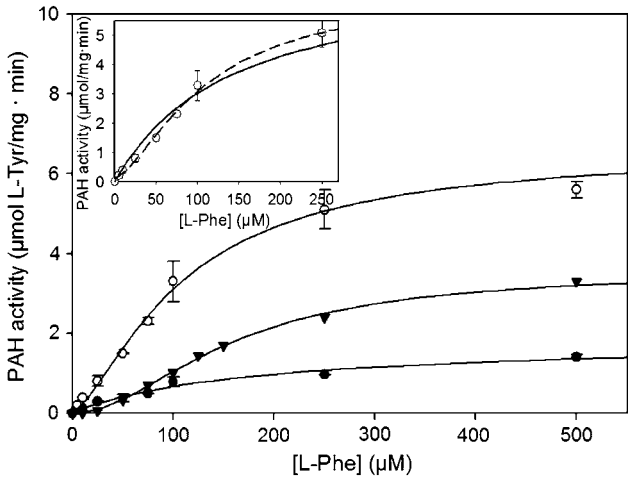

Fig. 4 Substrate dependence of the PAH activity. **a** The activity of hPAH as a function of the concentration of L-Phe, with fitting of the data to the Hill-equation (*triangle*), cePAH, with fitting to the Michaelis–Menten equation (*filled circle*) and Q215K/N216Y-cePAH, with fitting to the Hill-equation (*open circle*). *Inset* the substrate dependence of the activity of Q215K/N216Y-cePAH with fitting of the data to either the Hill equation ($h = 1.42$) (*dashed line*) or to the hyperbolic Michaelis–Menten equation (*continuous line*)

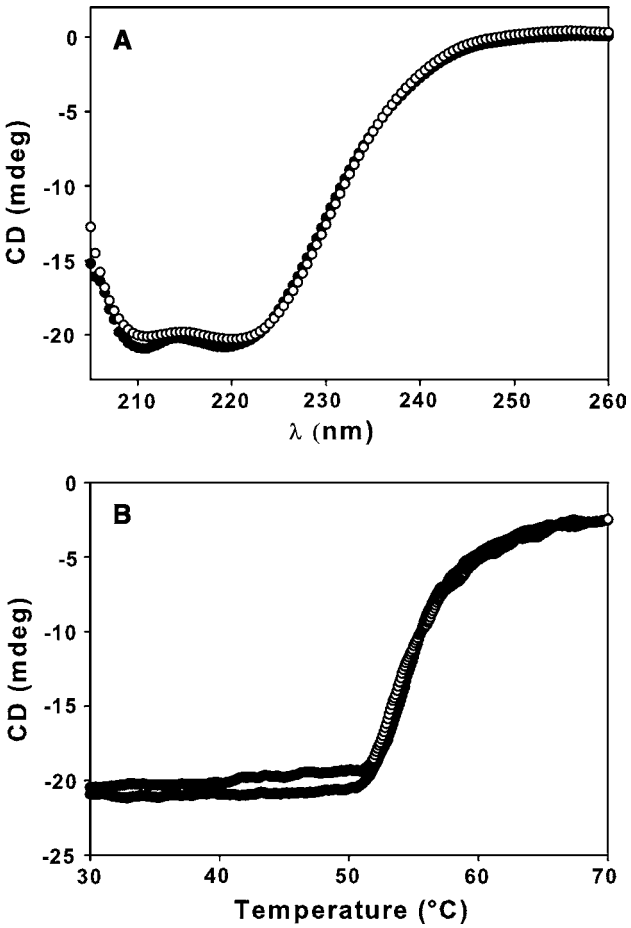

Fig. 5 Conformational stability of the cePAH proteins. The experiments were performed with cePAH (*filled circle*) and Q215K/N216Y-cePAH (*open circle*) in 20 mM Hepes, 200 mM NaCl, pH 7.0 using 5 μM subunit. **a** Far-UV CD spectra acquired at 25°C. **b** CD-monitored thermal denaturation at 222 nm, at 60°C/h scan rate

signal-to-noise ratios were obtained at a protein concentration of 30–40 μM subunit. Representative thermograms and isotherms for L-Phe binding at 25°C are shown in Fig. 6. While the binding of the cofactor BH_4 to hPAH at this temperature is strongly exothermic ($\Delta H = -11.8 \pm 0.4$ kcal/mol), ΔH is small (still negative) for the binding of L-Phe to cePAH and hPAH, and large for the mutant Q215K/N216Y-cePAH (Fig. 6). Fitting to one type of binding sites is satisfactory for the three binding isotherms. In the case of cePAH (but not the mutant Q215K/N216Y-cePAH and hPAH) the fittings of the ITC data also converge to a model for two sequential binding sites with somehow different binding constants (Table 2). The mutant shows a high affinity for L-Phe, with K_d-values that are lower than for cePAH or hPAH. This is in agreement with the lower $[S]_{0.5}$ obtained in the kinetic measurements for the mutant (Table 1). More interestingly, the values of the stoichiometry (n of L-Phe bound/subunit) for cePAH,

Q215K/N216Y-cePAH and hPAH were calculated to be 2.0, 1.4 and 1.2, respectively (Table 2).

Diverge analysis

Residues Lys215 and Tyr216 are conserved in all mammalian forms of PAH and TPHs and present a high degree of similarity in TH (Fig. 7). TH and the TPHs are not known to be regulated by amino acids, and secondary regulatory binding sites for their substrates have not been inferred. Lys215 and Tyr216 are not conserved in PAH of lower eukaryotes, which shows less voluminous substitutions at the corresponding positions. In fact, detailed diverge analyses clearly show functional divergence between nematode and mammalian PAH for these residues (Fig. 8a). Moreover, (KY)CG motif, where Lys215 and Tyr216 are included in mammals, is not present in the bacterial forms of PAH, which do not contain the regulatory ACT domain (Fig. 7). Thus, the (KY)CG motif is an indel in the catalytic domain located at the structural interface between the interacting regulatory and catalytic domains (see Fig. 8b for structural location), where it appears to be correlated with domain communication.

Discussion

The function of mammalian PAH has been investigated over many years due to its important role in the aromatic amino acid metabolism. The PAH reaction serves two main purposes. First, it is not only the initial and rate-limiting step in the L-Phe catabolism; it is also the only metabolic pathway by which L-Phe can be completely catabolized to carbon dioxide and water (Hufton et al. 1995; Scriver and Kaufman 2001). Second, it provides a continuous supply of tyrosine, which makes tyrosine a non-essential dietary amino acid (Hufton et al. 1995). The PAH catabolic pathway, which also includes the biosynthetic and regenerating enzymes of BH_4 (Thöny et al. 2000), accounts for more than 75% of the disposal of dietary phenylalanine. In order to avoid the neurological damage accompanying hyperphenylalaninemia, as seen in PKU, and to control the L-Phe levels in blood despite fluctuations in either L-Phe or L-Tyr levels due to diet (Scriver and Kaufman 2001), the mammalian enzymes rely on sophisticated regulatory mechanisms, such as the activation by L-Phe and a cooperative response of hPAH to substrate concentration.

Structural determinants for positive cooperativity: L-Phe binding at the regulatory domain

Despite the fact that the regulatory domain of hPAH contains the L-Phe binding motifs (GAL/IESRP) (Fig. 1) and that the substrate binds to the isolated regulatory ACT domain (Gjetting et al. 2001), detailed DSC titrations unequivocally demonstrated that full-length hPAH binds the substrate only at the catalytic domain, where it elicits the cooperative allosteric response (Thórólfsson et al.

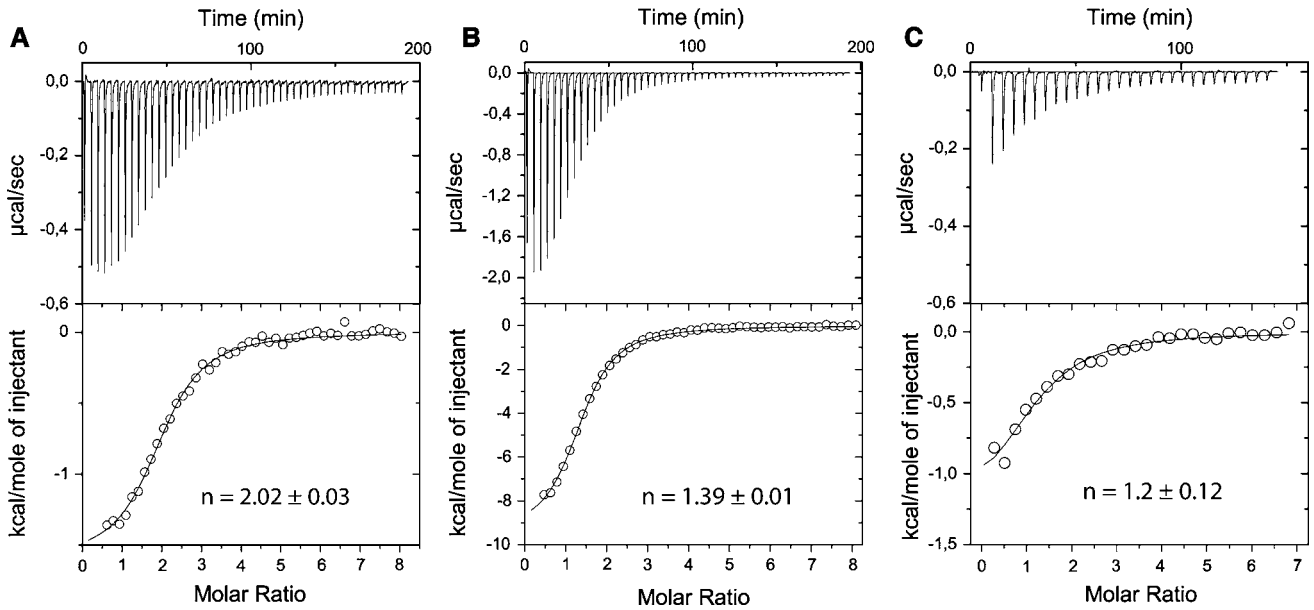

Fig. 6 Binding of L-Phe to PAH enzymes studied by ITC. *Upper panels* show thermograms for the binding of L-Phe to cePAH (**a**), Q215K/N216Y-cePAH (**b**) and hPAH (**c**) at 25°C and pH 7.0. Tetrameric cePAH (42 µM subunit), Q215K/N216Y-cePAH (30 µM subunit) and hPAH (28 µM subunit) were titrated with stock solutions of 0.9–2.0 mM L-Phe. *Lower panels* show the corresponding binding isotherms where each point represents the integrated heat of the associated peak in the thermogram. Fitting to one set of independent sites is shown. See also Table 2

Table 2 Thermodynamic parameters obtained by ITC for the binding of L-Phe to cePAH, Q215K/N216Y–cePAH and hPAH at 25°C

Enzyme	n	K_a (M^{-1})	K_d (μM)	ΔH (kcal/mol)	$-T\Delta S$ (kcal/mol)
cePAH[a]					
One set of binding sites	2.1 ± 0.05	(9.4 ± 1.0) × 10^4	10.6	−1.1 ± 0.1	−5.7
Two sequential binding sites	1	K_1 = (1.2 ± 0.1) × 10^5	8.2	−1.8 ± 0.07	−5.0
	1	K_2 = (6.7 ± 0.4) × 10^4	15.0	−1.3 ± 0.07	−5.2
Q215K/N216Y-cePAH[b]	1.4 ± 0.01	(17.4 ± 0.7) × 10^4	5.7	−8.8 ± 0.1	1.7
hPAH[b]	1.2 ± 0.10	(7.4 ± 1.8) × 10^4	13.6	−1.3 ± 0.2	−5.3

Data are mean ± SEM from fitting to representative experiments. Three or more independent experiments were performed with each enzyme

[a] Very similar fitting error (as measured by chi-square/degrees of freedom (χ^2/dof) values) was obtained for the fitting of the data for cePAH to either the model of one set of binding sites (χ^2/dof = 910–940) or two sequential binding sites (χ^2/dof = 900–1,000)

[b] One set of binding sites

2002). The present ITC results further confirm the stoichiometric binding of L-Phe to hPAH. On the other hand cePAH binds ~2 L-Phe per subunit, while in the humanized mutant Q215K/N216Y-cePAH the binding is reduced to $n \simeq 1.4$. This n-value seems to point to some L-Phe (~0.4 mol/mol subunit) still binding in regulatory binding sites which are not totally occluded by Lys and Tyr at the catalytic domain in the mutant. Nevertheless, Q215K/N216Y-cePAH shows a significant reduction in binding stoichiometry and approaches the n-value (=1.2) obtained by ITC for hPAH (Table 2). This result, combined with the structural analysis (Figs. 2, 3), supports that the residues Lys215/Tyr216 at the catalytic subunit in mammalian PAH act as closed gates and thereby inhibit L-Phe binding at the GAL/IESRP motifs in the regulatory domain from the adjacent subunit.

It is reasonable to assume that the mutant Q215K/N216Y-cePAH binds a stoichiometric amount of L-Phe at the catalytic site, and this binding certainly occurs with higher affinity than for wt-cePAH (Tables 1, 2; see also below). The higher affinity for L-Phe and the higher specific activity of the mutant indicate that this enzyme form is in an activated state compared with wt-cePAH. Interestingly, mutations that stabilize the interactions between regulatory and catalytic domains at adjacent subunits—as is the case for the Q215K/N216Y-cePAH mutant with respect to wt-cePAH—also activate hPAH (Thórólfsson et al. 2003). For mammalian PAH activation is also associated to an increase in the apparent size of the tetramer (Kappock et al. 1995; Kleppe et al. 1999) and, accordingly, the mutant shows an increased size compared with the wt-cePAH.

Like PAHs from other lower eukaryote organisms (Bel et al. 1992; Siltberg-Liberles et al. 2008), cePAH is not activated by preincubation with L-Phe and shows hyperbolic response to L-Phe concentration ($h \simeq 0.9$) (Calvo et al. 2008). The modest, but significant cooperative response exhibited by Q215K/N216Y-cePAH ($h \simeq 1.4$) indicates that the mutant has approached hPAH with regard to this important regulatory mechanism. Our results support that blocking L-Phe binding to the regulatory site might be related to the gain of positive cooperativity and allosteric communication between catalytic domains.

Regulation of hPAH and the cePAH enzymes

The differences in regulation of PAH activity between higher and lower eukaryotes are most likely a result of differences in requirements for L-Phe homeostasis. In the human body it is crucial to have a highly functional PAH system that responds promptly to increased levels of L-Phe to avoid damage of the brain (Scriver and Kaufman 2001). This system must also be inactivated at low L-Phe levels to maintain a minimum level of this essential amino acid for protein synthesis. Positive cooperativity serves all these needs. On the other hand, and although a catabolic function has been associated to PAH in *C. elegans* (Fisher et al. 2008), careful phenotype investigations on the knockout *pah-1* nematode have shown that cePAH has a major function related to the synthesis of a melanin-like pigment (Calvo et al. 2008). This also appears to be a main function in bacteria and other lower eukaryotes (Infanger et al. 2004; Leiros et al. 2007; Wiens et al. 1998). The evolutionary adaptation of PAH function from mainly anabolic in lower eukaryotes to highly regulated catabolic in mammals could derive from a progressive adaptation to a higher physiological—notably neurological—complexity.

ACT domains that bind amino acids often perform sophisticated allosteric regulation by cross talking from one ACT monomer to another in a higher oligomeric context (Kobe et al. 1999; Siltberg-Liberles and Martinez 2009). The amino acid binding capacity at the GAL/IESRP region in PAH (and PDT (Fig. 1)) might have been regulated by concerted changes at the interacting catalytic domain (KYCG) (Fig. 8). With these changes, the L-Phe binding function of the ACT domain of lower eukaryotes

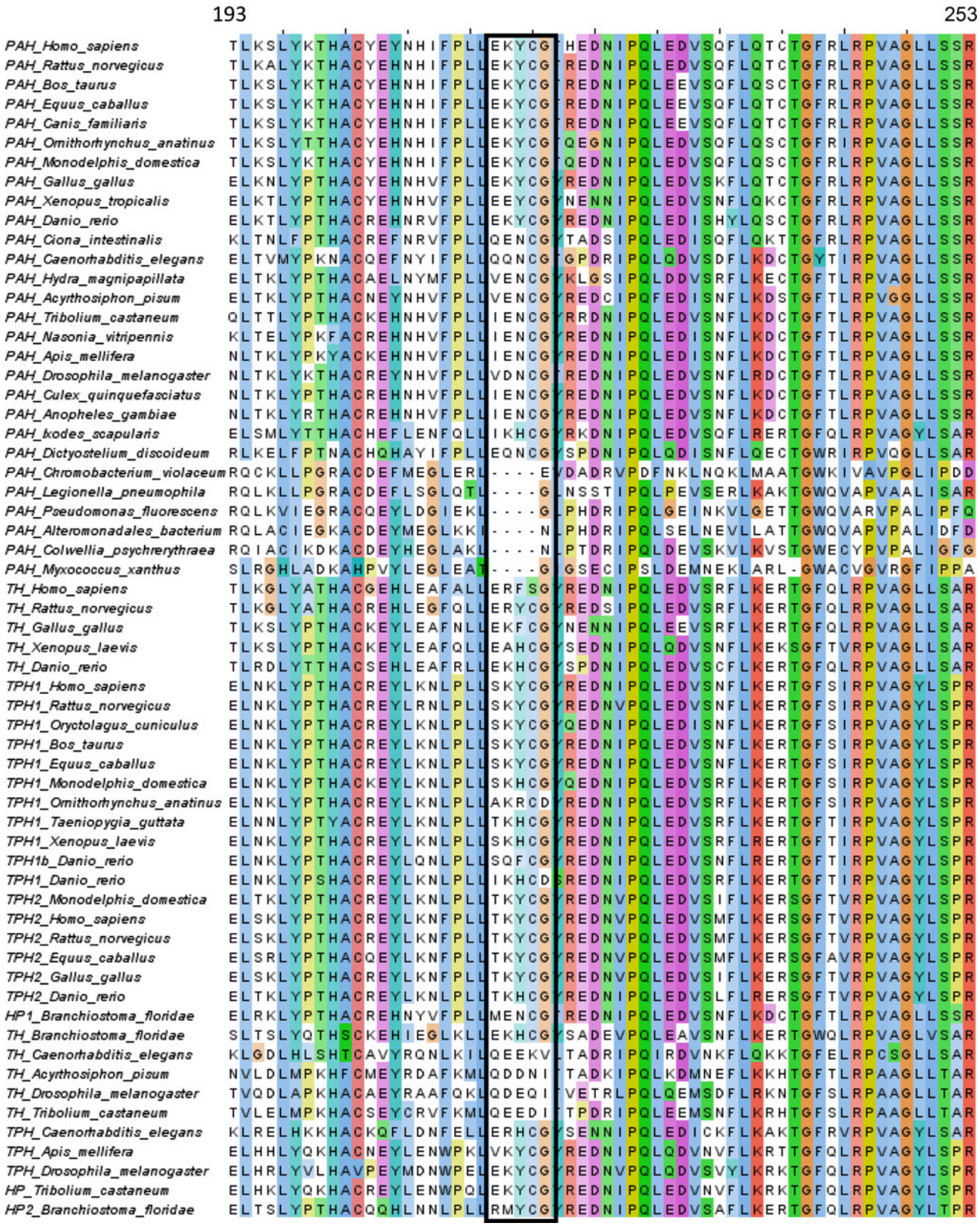
193
253
PAH_Homo_sapiens TLKSLYKTHACYEYNHIFPLLEKYCGFHEDNIPQLEDVSQFLQTCTGFRLRPVAGLLSSR
PAH_Rattus_norvegicus TLKALYKTHACYEHNHIFPLLEKYCGFREDNIPQLEDVSQFLQTCTGFRLRPVAGLLSSR
PAH_Bos_taurus TLKSLYKTHACYEHNHIFPLLEKYCGFREDNIPQLEEVSQFLQSCTGFRLRPVAGLLSSR
PAH_Equus_caballus TLKSLYKTHACYEHNHIFPLLEKYCGFREDNIPQLEEVSQFLQTCTGFRLRPVAGLLSSR
PAH_Canis_familiaris TLKSLYKTHACYEHNHIFPLLEKYCGFREDNIPQLEEVSQFLQTCTGFRLRPVAGLLSSR
PAH_Ornithorhynchus_anatinus TLKSLYTTHACYEHNHIFPLLEKYCGFQEGNIPQLEDVSQFLQSCTGFRIRPVAGLLSSR
PAH_Monodelphis_domestica TLKSLYKTHACYEHNHIFPLLEKYCGFQEDNIPQLEDVSQFLQSCTGFRLRPVAGLLSSR
PAH_Gallus_gallus ELKNLYPTHACYEHNHVFPLLEKYCGYREDNIPQLEDVSKFLQTCTGFRLRPVAGLLSSR
PAH_Xenopus_tropicalis ELKTLYPTHACYEHNHVFPLLEEYCGYNENNIPQLEDVSNFLQKCTGFRLRPVAGLLSSR
PAH_Danio_rerio ELKTLYPTHACREHNRVFPLLEKYCGYREDNIPQLEDISHYLQSCTGFRLRPVAGLLSSR
PAH_Ciona_intestinalis KLTNLFPTHACREFNRVFPLLQENCGYTADSIPQLEDISQFLQKTTGFRLRPVAGLLSSR
PAH_Caenorhabditis_elegans ELTVMYPKNACQEFNYIFPLLQQNCGFGPDRIPQLQDVSDFLKDCTGYTIRPVAGLLSSR
PAH_Hydra_magnipapillata ELTKLYPTHACAELNYMFPLLVENCGYKLGSIPQLDDVSRFLKECTGFTLRPVAGLLSSR
PAH_Acyrthosiphon_pisum ELTKLYPTHACNEYNHVFPLLVENCGYREDCIPQFEDISNFLKDSTGFTLRPVGGLLSSR
PAH_Tribolium_castaneum QLTTLYPTHACKEHNHVFPLLIENCGYRRDNIPQLEDVSNFLKDCTGFTLRPVAGLLSSR
PAH_Nasonia_vitripennis KLTELYPKFACREHNHVFPLLIENCGYREDNIPQLEDISNFLKDCTGFTLRPVAGLLSSR
PAH_Apis_mellifera NLTKLYPKYACKEHNHVFPLLIENCGYREDNIPQLEDISNFLKDCTGFTLRPVAGLLSSR
PAH_Drosophila_melanogaster NLTKLYKTHACREYNHVFPLLVDNCGFREDNIPQLEDVSNFLRDCTGFTLRPVAGLLSSR
PAH_Culex_quinquefasciatus NLTKLYPTHACREHNHVFPLLIENCGYREDNIPQLEDVSNFLKDCTGFTLRPVAGLLSSR
PAH_Anopheles_gambiae NLTKLYRTHACREHNHVFPLLIENCGYREDNIPQLEDVSNFLKDCTGFTLRPVAGLLSSR
PAH_Ixodes_scapularis ELSMLYTTHACHEFLENFQLLIKHCGYRKDNIPQLEDVSQFLRERTGFQLRPVAGYLSAR
PAH_Dictyostelium_discoideum RLKELFPTNACHQHAYIFPLLEQNCGYSPDNIPQLQDISNFLQECTGWRIRPVQGLLSAR
PAH_Chromobacterium_violaceum RQCKLLPGRACDEFMEGLERL----EVDADRVPDFNKLNQKLMAATGWKIVAVPGLIPDD
PAH_Legionella_pneumophila RQLKLLPGRACDEFLSGLQTL----GLNSSTIPQLPEVSERLKAKTGWQVAPVAALISAR
PAH_Pseudomonas_fluorescens RQLKVIEGRACQEYLDGIEKL----GLPHDRIPQLGEINKVLGETTGWQVARVPALIPFQ
PAH_Alteromonadales_bacterium RQLACIEGKACDEYMEGLKKI----NLPHDRIPQLSELNEVLLATTGWQVAPVPALIDFD
PAH_Colwellia_psychrerythraea RQIACIKDKACDEYHEGLAKL----NLPTDRIPQLDEVSKVLKVSTGWECYPVPALIGFG
PAH_Myxococcus_xanthus SLRGHLADKAHPVYLEGLEAT----GGSECIPSLDEMNEKLARL-GWACVGVRGFIPPA
TH_Homo_sapiens TLKGLYATHACGEHLEAFALLERFSGYREDNIPQLEDVSRFLKERTGFQLRPVAGLLSAR
TH_Rattus_norvegicus TLKGLYATHACREHLEGFQLLERYCGYREDSIPQLEDVSRFLKERTGFQLRPVAGLLSAR
TH_Gallus_gallus TLKSLYPTHACKEYLEAFNLLEKFCGYNENNIPQLEEVSRFLKERTGFQLRPVAGLLSAR
TH_Xenopus_laevis TLKSLYPTHACKEYLEAFQLLEAHCGYSEDNIPQLQDVSNFLKEKSGFTVRPVAGLLSAR
TH_Danio_rerio TLRDLYTTHACSEHLEAFRLLEKHCGYSPDNIPQLEDVSCFLKERTGFQLRPVAGLLSAR
TPH1_Homo_sapiens ELNKLYPTHACREYLKNLPLLSKYCGYREDNIPQLEDVSNFLKERTGFSIRPVAGYLSPR
TPH1_Rattus_norvegicus ELNKLYPTHACREYLRNLPLLSKYCGYREDNVPQLEDVSNFLKERTGFSIRPVAGYLSPR
TPH1_Oryctolagus_cuniculus ELNKLYPTHACREYLKNLPLLSKYCGYQEDNIPQLEDISNFLKERTGFSIRPVAGYLSPR
TPH1_Bos_taurus ELNKLYPTHACREYLKNLPLLSKYCGYREDNIPQLEDVSNFLKERTGFSIRPVAGYLSPR
TPH1_Equus_caballus ELNKLYPTHACREYLKNLPLLSKYCGYREDNIPQLEDVSNFLKERTGFSIRPVAGYLSPR
TPH1_Monodelphis_domestica ELNKLYPTHACKEYLKNLPLLSKHCGYQEDNIPQLEDVSRFLKERTGFSIRPVAGYLSPR
TPH1_Ornithorhynchus_anatinus ELNKLYPTHACREYLKNLPLLAKRCDYREDNIPQLEDVSRFLKERTGFSIRPVAGYLSPR
TPH1_Taeniopygia_guttata ELNNLYPTYACREYLKNLPLLTKHCGYREDNIPQLEDVSRFLKERTGFTIRPVAGYLSPR
TPH1_Xenopus_laevis ELNKLYPTHACREYLKNLPLLSKHCGYREDNIPQLEDVSRFLRERTGFTIRPVAGYLSPR
TPH1b_Danio_rerio ELNKLYPTHACREYLQNLPLLSQFCGYREDNIPQLEDVSNFLRERTGFTIRPVAGYLSPR
TPH1_Danio_rerio ELNKLYPSHACREYLKNLPLLIKHCDSREDNIPQLEDVSRFLKERTGFTIRPVAGYLSPR
TPH2_Monodelphis_domestica ELTKLYPTHACREYLKNLPLLTKYCGYREDNVPQLEDVSIFLKERSGFTVRPVAGYLSPR
TPH2_Homo_sapiens ELSKLYPTHACREYLKNFPLLTKYCGYREDNVPQLEDVSMFLKERSGFTVRPVAGYLSPR
TPH2_Rattus_norvegicus ELSKLYPTHACREYLKNFPLLTKYCGYREDNVPQLEDVSMFLKERSGFTVRPVAGYLSPR
TPH2_Equus_caballus ELSRLYPTHACQEYLKNFPLLTKYCGYREDNVPQLEDVSMFLKERSGFAVRPVAGYLSPR
TPH2_Gallus_gallus ELSKLYPTHACREYLKNFPLLTKYCGYREDNVPQLEDVSIFLKERSGFTVRPVAGYLSPR
TPH2_Danio_rerio ELTKLYPTHACREYLKNLPLLTKHCGYREDNIPQLEDVSLFLRERSGFTVRPVAGYLSPR
HP1_Branchiostoma_floridae ELRKLYPTHACREHNYVFPLLMENCGFREDNIPQLEDVSNFLKDCTGFTLRPVAGLLSSR
TH_Branchiostoma_floridae SLTSLYQTHSCKEHIEGLKLLEKHCGYSADEVPQLEAVSNFLKERTGWQLRPVAGLVSAR
TH_Caenorhabditis_elegans KLGDLHLSHTCAVYRQNLKILQEEKVLTADRIPQIRDVNKFLQKKTGFELRPCSGLLSAR
TH_Acyrthosiphon_pisum NVLDLMPKHFCMEYRDAFKMLQDDNITTADKIPQLKDMNEFLKKHTGFTLRPAAGLLTAR
TH_Drosophila_melanogaster TVQDLAPKHACAEYRAAFQKLQDEQITVETRLPQLQEMSDFLRKNTGFSLRPAAGLLTAR
TH_Tribolium_castaneum TVLELMPKHACSEYCRVFKMLQEEDITTPDRIPQLEEMSNFLKRHTGFSLRPAAGLLTAR
TPH_Caenorhabditis_elegans KLRELHKKHACKQFLDNFELLERHCGYSENNIPQLEDICKFLKAKTGFRVRPVAGYLSAR
TPH_Apis_mellifera ELHHLYQKHACNEYLENWPKLVKYCGYREDNIPQLQDVNVFLKRTTGFQLRPVAGYLSPR
TPH_Drosophila_melanogaster ELHRLYVLHAVPEYMDNWPELEKYCGYREDNVPQLQDVSVYLKRKTGFQLRPVAGYLSPR
HP_Tribolium_castaneum ELHKLYQKHACREYLENWPQLEKYCGYREDNIPQLEDVNVFLKRKTGFQLRPVAGYLSPR
HP2_Branchiostoma_floridae ELTSLYPTHACQQHLNNLPLLRMYCGYREDNIPQLEDVSAFLKERTGFQLRPVAGYLTPR

◄ **Fig. 7** The (KY)CG motif in the AAAH superfamily context. Sequence alignment around Lys215 and Tyr216 (numeration in hPAH) prepared with Muscle (Edgar 2004) and rendered in JalView (Clamp et al. 2004). The motif is located in an area with fairly conserved amino acid sequence. Most vertebrate PAH sequences have the KY residues in the (KY)CG motif (within the *black box*), which is changed to (Q/E/D,N)CG in most metazoan invertebrates and protozoan. The (KY)CG motif is absent in the bacterial PAHs, which only contain the catalytic domain. The (KY)CG motif is rather conserved in the TPH sequences, but not in the THs. The following sequences were used gil71980736, gil115533973, gil119471173, gil77457726, gil54295485, gil34498635, gil108757987, gil71279120, gil4557819, gil149742972, gil114051455, gil158262033, gil73978257, gil126339754, gil149637901, gil47604920, gil73853802, gil41054599, gil24660393, gil91092806, gil198437597, gil156552627, gil170031082, gil193591716, gil221119662, gil17531391, gil126332093, gil47604924, gil31795563, gil126339369, gil119907190, gil149585793, gil4759248, gil158186610, gil30231266, gil149719489, gil148237026, gil27753970, gil126352616, gil125630300, gil153791957, gil241034174, gil66815885, gil91079871, gil66512299, gil6981652, gil47550885, gil88900503, gil24654994, gil169234748, gil45382205, gil17136774, gil149588788, gil193652543, gil66501322, gil158294628, gil147904126, gil224050838, gil219493294, gil71553713 and gil219427784

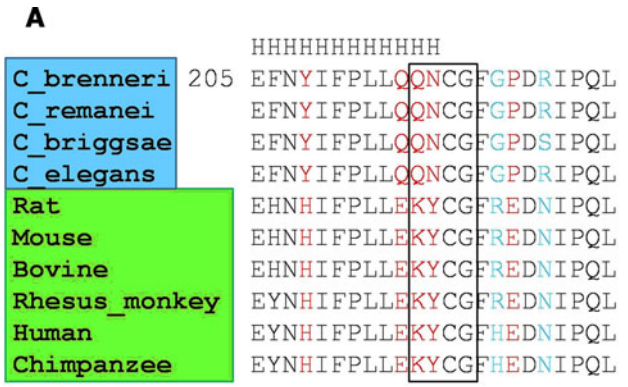

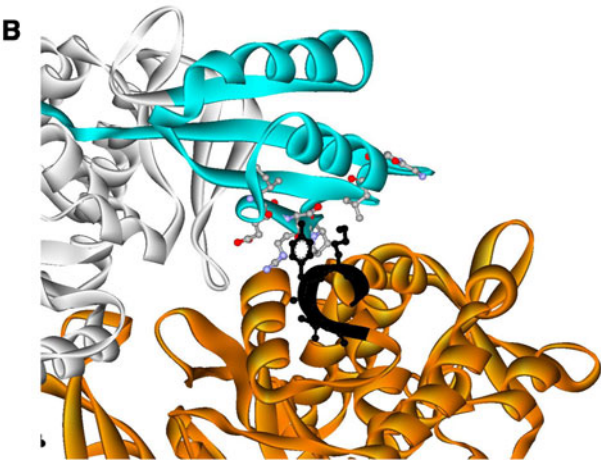

Fig. 8 Diverge prediction of type II functional divergence. **a** Diverge analysis between PAH from the nematode clade (*blue*) and mammalian clade (*green*) of the area surrounding the residues mutated in this study. Sites with clade-specific radical changes (*red*) and sites with radical changes between the clade allowing some within-cluster variation (*turquoise*) are marked on the alignment. The nematode clade included *C. brenneri* (gb_ABEG010099771), *C. remanei* (gb_AAGD020003811), *C. briggsae* (gil39597500) and *C. elegans* (gil17531391). The mammalian clade included rat (gil6981330), mouse (gil6679203), bovine (gil114051455), Rhesus macaque (gil109098481), human (gil4557819) and chimpanzee (gil1146-46573). **b** Detailed view of the ACT regulatory domain of rat PAH, in *blue*, with the residues in the GAL/IESRP motifs in stick representation. The catalytic domain of the adjacent subunit in the dimer is shown in *light brown*, with the region E214-KYCG-F219 in *black*. The residues KYCG (corresponding to the insertion found in hPAH comparative to bacterial PAHs (Fig. 7) and to QNCG in cePAH) are shown in *ball* and *stick* representation. Note that the insertion constitutes a turn at the end of the α-helix, with Tyr216 blocking the putative binding site for L-Phe at the GAL/IERSP motifs in the regulatory domain (color figure online)

may adapt in mammals to a role in which the domain participates in transmission of cooperative conformational changes, as indicated by mutagenesis and molecular dynamics simulations (Thórólfsson et al. 2003). While positive cooperativity appears as an optimal mechanism to maintain homeostasis in mammals in parallel to the development of a complex mammalian nervous system which should be protected from elevated L-Phe concentrations and PKU (Kappock and Caradonna 1996; Kaufman 1993; Scriver and Kaufman 2001), the need for a secondary regulatory binding site in cePAH—and most probably in other lower eukaryotes (Fig. 7)—does not appear so clear. One might speculate that binding of L-Phe to the non-catalytic site might preserve a threshold value of L-Phe for protein synthesis, ensuring that it is not completely depleted by conversion to L-Tyr at the active site, and/or would safeguard a correct catalytic conformation for the cePAH tetramer. These functions would require a binding site with a higher affinity for L-Phe than the catalytic site. The regulatory site could thus very well correspond to the site with a $K_d = 8.2$ μM revealed by the fitting of the binding data to a two-binding sites model, while the site with $K_d = 15$ μM (very similar to the value for hPAH (Table 2)) would correspond to the catalytic site.

In conclusion, this work has revealed significant differences between PAH from human and *C. elegans* with regards to the stoichiometry of L-Phe binding and allosteric regulation. Our results point to two different regulatory mechanisms which appear to accompany eukaryote PAH function: (i) L-Phe binding at a regulatory site different to the catalytic site, and (ii) allosteric-positive cooperativity. These mechanisms would, respectively, correspond to the regulation of functions that are mainly anabolic (in lower eukaryotes) (Calvo et al. 2008) or catabolic (in mammals) (Scriver and Kaufman 2001). Our results, thus, contribute to the understanding of the evolutionary adaptation of PAH.

Acknowledgments The expert assistance of Randi M. Svebak and Ali J. Muñoz Sepulveda is greatly appreciated. We are grateful to Anne Wiemhoefer and Thies Nolte for preliminary DSC experiments. This work received support from the Research Council of Norway and Meltzer L. Høyskolefond.

References

An J, Totrov M, Abagyan R (2005) Pocketome via comprehensive identification and classification of ligand binding envelopes. Mol Cell Proteomics 4:752–761

Bel Y, Jacobson KB, Ferre J (1992) A comparative study of Drosophila phenylalanine hydroxylase with a natural and a synthetic tetrahydropterin as cofactor. Comp Biochem Physiol B 103:557–562

Calvo AC, Pey AL, Ying M, Loer CM, Martinez A (2008) Anabolic function of phenylalanine hydroxylase in *Caenorhabditis elegans*. FASEB J 22:3046–3058

Case DA, Darden TA, Cheatham TE I, Simmerling CL, Wang J, Duke RE et al (2008) AMBER 10. University of California, San Francisco

Clamp M, Cuff J, Searle SM, Barton GJ (2004) The Jalview Java alignment editor. Bioinformatics 20:426–427

Døskeland AP, Døskeland SO, Øgreid D, Flatmark T (1984) The effect of ligands of phenylalanine 4-monooxygenase on the cAMP-dependent phosphorylation of the enzyme. J Biol Chem 259:11242–11248

Edgar RC (2004) MUSCLE: multiple sequence alignment with high accuracy and high throughput. Nucl Acids Res 32:1792–1797

Erlandsen H, Pey AL, Gamez A, Perez B, Desviat LR, Aguado C et al (2004) Correction of kinetic and stability defects by tetrahydrobiopterin in phenylketonuria patients with certain phenylalanine hydroxylase mutations. Proc Natl Acad Sci USA 101:16903–16908

Fisher AL, Page KE, Lithgow GJ, Nash L (2008) The *Caenorhabditis elegans* K10C2.4 gene encodes a member of the fumarylacetoacetate hydrolase family: a *Caenorhabditis elegans* model of type I tyrosinemia. J Biol Chem 283:9127–9135

Fitzpatrick PF (1999) Tetrahydropterin-dependent amino acid hydroxylases. Annu Rev Biochem 68:355–381

Fitzpatrick PF (2003) Mechanism of aromatic amino acid hydroxylation. Biochemistry 42:14083–14091

Flatmark T, Stevens RC (1999) Structural insight into the aromatic amino acid hydroxylases and their disease-related mutant forms. Chem Rev 99:2137–2160

Gersting SW, Kemter KF, Staudigl M, Messing DD, Danecka MK, Lagler FB et al (2008) Loss of function in phenylketonuria is caused by impaired molecular motions and conformational instability. Am J Hum Genet 83:5–17

Gjetting T, Petersen M, Guldberg P, Guttler F (2001) Missense mutations in the N-terminal domain of human phenylalanine hydroxylase interfere with binding of regulatory phenylalanine. Am J Hum Genet 68:1353–1360

Gu X (2001) Maximum-likelihood approach for gene family evolution under functional divergence. Mol Biol Evol 18:453–464

Gu X (2006) A simple statistical method for estimating type-II (cluster-specific) functional divergence of protein sequences. Mol Biol Evol 23:1937–1945

Hooft RW, Vriend G, Sander C, Abola EE (1996) Errors in protein structures. Nature 381:272

Hufton SE, Jennings IG, Cotton RG (1995) Structure and function of the aromatic amino acid hydroxylases. Biochem J 311:353–366

Infanger LC, Rocheleau TA, Bartholomay LC, Johnson JK, Fuchs J, Higgs S et al (2004) The role of phenylalanine hydroxylase in melanotic encapsulation of filarial worms in two species of mosquitoes. Insect Biochem Mol Biol 34:1329–1338

Kappock TJ, Caradonna JP (1996) Pterin-dependent amino acid hydroxylases. Chem Rev 96:2659–2756

Kappock TJ, Harkins PC, Friedenberg S, Caradonna JP (1995) Spectroscopic and kinetic properties of unphosphorylated rat hepatic phenylalanine hydroxylase expressed in *Escherichia coli*—comparison of resting and activated states. J Biol Chem 270:30532–30544

Kaufman S (1993) The phenylalanine hydroxylating system. Adv Enzymol Relat Areas Mol Biol 67:77–264

Kleppe R, Uhlemann K, Knappskog PM, Haavik J (1999) Urea-induced denaturation of human phenylalanine hydroxylase. J Biol Chem 274:33251–33258

Kobe B, Jennings IG, House CM, Michell BJ, Goodwill KE, Santarsiero BD et al (1999) Structural basis of autoregulation of phenylalanine hydroxylase. Nat Struct Biol 6:442–448

Leiros HK, Pey AL, Innselset M, Moe E, Leiros I, Steen IH et al (2007) Structure of phenylalanine hydroxylase from *Colwellia psychrerythraea* 34H, a monomeric cold active enzyme with local flexibility around the active site and high overall stability. J Biol Chem 282:21973–21986

Loer CM, Davidson B, McKerrow J (1999) A phenylalanine hydroxylase gene from the nematode *C. elegans* is expressed in the hypodermis. J Neurogenet 13:157–180

Martínez A, Haavik J, Flatmark T (1990) Cooperative homotropic interaction of L-noradrenaline with the catalytic site of phenylalanine 4-monooxygenase. Eur J Biochem 193:211–219

Martínez A, Olafsdottir S, Flatmark T (1993) The cooperative binding of phenylalanine to phenylalanine 4-monooxygenase studied by 1H-NMR paramagnetic relaxation. Changes in water accessibility to the iron at the active site upon substrate binding. Eur J Biochem 211:259–266

Pey AL, Thórólfsson M, Teigen K, Ugarte M, Martínez A (2004) Thermodynamic characterization of the binding of tetrahydropterins to phenylalanine hydroxylase. J Am Chem Soc 126:13670–13678

Phillips RS, Kaufman S (1984) Ligand effects on the phosphorylation state of hepatic phenylalanine hydroxylase. J Biol Chem 259:2474–2479

Schwede T, Kopp J, Guex N, Peitsch MC (2003) SWISS-MODEL: an automated protein homology-modeling server. Nucl Acids Res 31:3381–3385

Scriver CR, Kaufman S (2001) Hyperphenylalaninemia:phenylalanine hydroxylase deficiency. In: Scriver CR, Beaudet AL, Valle D, Sly WS (eds) The metabolic and molecular bases of inherited disease, 8th edn. McGraw-Hill, New York, pp 1667–1724

Shiman R, Gray DW (1980) Substrate activation of phenylalanine hydroxylase. A kinetic characterization. J Biol Chem 255:4793–4800

Shiman R, Gray DW, Pater A (1979) A simple purification of phenylalanine hydroxylase by substrate-induced hydrophobic chromatography. J Biol Chem 254:11300–11306

Shiman R, Xia T, Hill MA, Gray DW (1994) Regulation of rat liver phenylalanine hydroxylase. II. Substrate binding and the role of activation in the control of enzymatic activity. J Biol Chem 269:24647–24656

Siltberg-Liberles J, Martinez A (2009) Searching distant homologs of the regulatory ACT domain in phenylalanine hydroxylase. Amino Acids 36:235–249

Siltberg-Liberles J, Steen IH, Svebak RM, Martinez A (2008) The phylogeny of the aromatic amino acid hydroxylases revisited by characterizing phenylalanine hydroxylase from *Dictyostelium discoideum*. Gene 427:86–92

Solstad T, Stokka AJ, Andersen OA, Flatmark T (2003) Studies on the regulatory properties of the pterin cofactor and dopamine bound at the active site of human phenylalanine hydroxylase. Eur J Biochem 270:981–990

Stokka AJ, Flatmark T (2003) Substrate-induced conformational transition in human phenylalanine hydroxylase as studied by surface plasmon resonance analyses: the effect of terminal deletions, substrate analogues and phosphorylation. Biochem J 369:509–518

Stokka AJ, Carvalho RN, Barroso JF, Flatmark T (2004) Probing the role of crystallographically defined/predicted hinge-bending regions in the substrate-induced global conformational transition and catalytic activation of human phenylalanine hydroxylase by single-site mutagenesis. J Biol Chem 279:26571–26580

Tan K, Li H, Zhang R, Gu M, Clancy ST, Joachimiak A (2008) Structures of open (R) and close (T) states of prephenate dehydratase (PDT)–implication of allosteric regulation by L-phenylalanine. J Struct Biol 162:94–107

Teigen K, McKinney JA, Haavik J, Martinez A (2007) Selectivity and affinity determinants for ligand binding to the aromatic amino Acid hydroxylases. Curr Med Chem 14:455–467

Thöny B, Auerbach G, Blau N (2000) Tetrahydrobiopterin biosynthesis, regeneration and functions. Biochem J 347(Pt 1):1–16

Thórólfsson M, Ibarra-Molero B, Fojan P, Petersen SB, Sanchez-Ruiz JM, Martínez A (2002) L-phenylalanine binding and domain organization in human phenylalanine hydroxylase: a differential scanning calorimetry study. Biochemistry 41:7573–7585

Thórólfsson M, Teigen K, Martínez A (2003) Activation of phenylalanine hydroxylase: effect of substitutions at Arg68 and Cys237. Biochemistry 42:3419–3428

Vriend G (1990) WHAT IF: a molecular modeling and drug design program. J Mol Graph 8:52–56

Wiens M, Koziol C, Batel R, Muller WE (1998) Phenylalanine hydroxylase from the sponge *Geodia cydonium*: implication for allorecognition and evolution of aromatic amino acid hydroxylases. Dev Comp Immunol 22:469–478